



Surface functionalized mesoporous polydopamine nanocomposites for killing tumor cells through collaborative chemo/photothermal/chemodynamic treatment

Yi Ouyang, Yan Chen[†], Ting Xu[†], Yihao Sun[†], Sheng Zhao[†], Chunmei Chen[†], Yixin Tan[†], Liang He[†], Hui Liu^{*ID}

Key Laboratory of Luminescence Analysis and Molecular Sensing (Southwest University), Ministry of Education, School of Materials and Energy, Chongqing 400715, China

[†]These authors contributed equally to this work.

***Correspondence:** Hui Liu, Key Laboratory of Luminescence Analysis and Molecular Sensing (Southwest University), Ministry of Education, School of Materials and Energy, Southwest University, Chongqing 400715, China. liuhui2016@swu.edu.cn

Academic Editor: Fernando Albericio, University of KwaZulu-Natal, South Africa; University of Barcelona, Spain

Received: October 26, 2022 **Accepted:** December 7, 2022 **Published:** February 27, 2023

Cite this article: Ouyang Y, Chen Y, Xu T, Sun Y, Zhao S, Chen C, et al. Surface functionalized mesoporous polydopamine nanocomposites for killing tumor cells through collaborative chemo/photothermal/chemodynamic treatment. *Explor Drug Sci.* 2023;1:18–30. <https://doi.org/10.37349/eds.2023.00003>

Abstract

Aim: The development of a collaborative strategy with improved efficacy holds great promise in tumor treatment. This study aims to develop an effective collaborative strategy based on functionalized mesoporous polydopamine (MPDA) nanocomposites for killing tumor cells.

Methods: MPDA nanoparticles were synthesized and functionalized with camptothecin (CPT) payload and manganese dioxide (MnO₂) coating to construct MPDA-CPT-MnO₂ nanocomposites.

Results: When uptaken by tumor cells, the nanocomposites can degrade to produce O₂, release CPT, and generate manganese (Mn²⁺) under the stimulation of hydrogen peroxide (H₂O₂) and acid. The released CPT and Mn²⁺ can act as chemotherapeutic drug and Fenton-like agent, respectively. Abundant reactive oxygen species (ROS) are generated in 4T1 tumor cells through an Mn²⁺-mediated Fenton-like reaction. After that, the generated Mn⁴⁺ can react with glutathione (GSH) through redox reaction to produce Mn²⁺ and deplete GSH, disrupting the reducing capacity and benefiting the production of ROS in tumor cells. Under laser irradiation, the nanocomposites can generate hyperthermia to promote the production of ROS.

Conclusions: The developed MPDA-CPT-MnO₂ nanocomposites can kill tumor cells through collaborative chemo/photothermal/chemodynamic therapy (CDT).

Keywords

Mesoporous polydopamine, chemotherapy, photothermal therapy, chemodynamic therapy, tumor treatment

Introduction

Photothermal therapy (PTT) is a type of tumor therapeutic method that involves artificially elevating local tissue temperature under near-infrared (NIR) light irradiation [1–6]. Due to its high inherent specificity

© The Author(s) 2023. This is an Open Access article licensed under a Creative Commons Attribution 4.0 International License (<https://creativecommons.org/licenses/by/4.0/>), which permits unrestricted use, sharing, adaptation, distribution and reproduction in any medium or format, for any purpose, even commercially, as long as you give appropriate credit to the original author(s) and the source, provide a link to the Creative Commons license, and indicate if changes were made.



and minimal intrusive burden, PTT is appealing in comparison to conventional tumor treatment techniques such as surgery, radiation, and chemotherapy (CT) [7, 8]. However, its treatment efficacy is limited by the conversion efficiency of photothermal agents (PTAs) and the penetration depth of NIR light [9, 10]. Combining PTT with other treatment techniques to construct multimodal treatment strategy holds great promise [11, 12]. For example, various chemotherapeutic drug delivery systems based on PTAs have been developed, showing synergistic effects between PTT and CT [13–19].

Among extensively explored chemotherapeutic drugs, camptothecin (CPT) is a hydrophobic plant alkaloid extracted from *Camptotheca acuminata*, which can damage the DNA of tumor cells [20–22]. CPT inhibits topoisomerase I and forms irreversible covalent compounds with it, leading to DNA double-strand breaks and inducing cell apoptosis [23]. Nonetheless, its clinical application has been hampered by poor water solubility, high systemic toxicity, hydrolysis inactivation, and so on [24, 25]. Therefore, it is necessary to design a drug delivery system to deliver CPT to tumor cells specifically [26, 27].

The nanocomposites that own photothermal conversion performance and drug loading capacity hold the potential to develop a synergistic CT/PTT strategy. As synthetic analogs of the naturally occurring eumelanin, mesoporous polydopamine (MPDA) is a kind of popular drug carrier due to its simple preparation method, good biocompatibility, high drug loading efficiency, and easy surface modification [28, 29]. Furthermore, the great photothermal conversion ability of MPDA makes it an excellent candidate for PTT [30, 31]. When delivering drugs, the pores on the MPDA surface should be blocked to avoid the leakage of drugs [32, 33]. Manganese dioxide (MnO_2) nanostructures own good pH-responsive performance and can be degraded under acid stimulation, showing great potential in tumor therapy [34–37]. At a low pH condition, the MnO_2 nanostructure can be rapidly broken, acting as a pH-responsive drug carrier or sealer for mesoporous nanomaterials [38, 39]. The unique reaction between MnO_2 and hydrogen peroxide (H_2O_2) can generate O_2 , alleviating the drug resistance of tumor cells to enhance the CT effect [40, 41]. In addition, manganese (Mn^{2+}) is a Fenton-like agent that can catalyze H_2O_2 to generate hydroxyl radicals ($\cdot\text{OH}$) for tumor chemodynamic therapy (CDT), which is a promising tumor therapy method [42–44]. The formation of $\text{Mn}^{2+}(\text{HCO}_3^-)_2$ complex is essential for Mn^{2+} ions to play the role of Fenton-like agents [45].

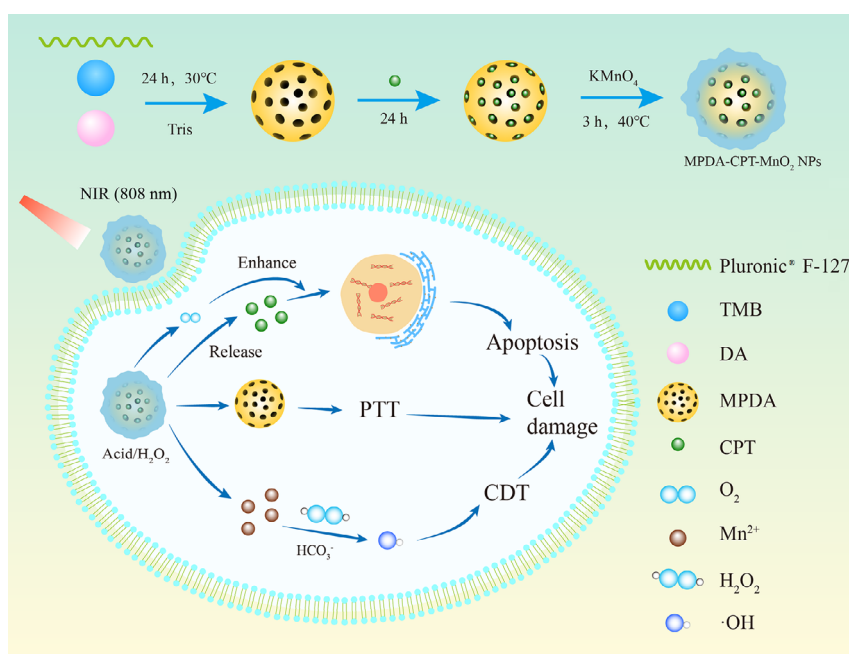


Figure 1. Schematic representation of the formation process of MPDA-CPT- MnO_2 nanocomposites and the mechanism for tumor cell killing through synergistic CT/PTT/CDT strategy. DA: dopamine; KMnO_4 : potassium permanganate; NPs: nanoparticles; Pluronic® F-127: poly(ethylene glycol)-*block*-poly(propylene glycol)-*block*-poly(ethylene glycol); TMB: 1,3,5-trimethylbenzene; \rightarrow : reaction process

Herein, an effective collaborative strategy based on functionalized MPDA nanocomposites was designed and developed for killing tumor cells (Figure 1). MPDA nanoparticles were prepared as the carrier to load the chemotherapeutic drug CPT and then coated with MnO_2 layer on the surface through the *in situ* redox

reaction between KMnO_4 and MPDA, finally obtaining MPDA-CPT- MnO_2 nanocomposites. When up-taken by tumor cells, the outer layer of MnO_2 reacts with H_2O_2 to generate O_2 and Mn^{2+} . In the presence of HCO_3^- , Mn^{2+} undergoes a Fenton-like reaction to produce $\cdot\text{OH}$ [46], which breaks the redox balance to cause tumor cell damage. After the MnO_2 coating is destroyed, the chemotherapeutic drug CPT is released from MPDA nanoparticles to cause cell apoptosis. Under laser irradiation, hyperthermia is generated by MPDA for PTT. Compared with the reported studies, this study developed a kind of rationally designed nanocomposites to realize collaborative CT/PTT/CDT against tumor cells.

Materials and methods

Materials

Tris (hydroxymethyl) aminomethane (Tris, 99.9%, CAS: 77-86-1) was purchased from Damas-beta. Dopamine hydrochloride (98%, AR, CAS: 62-31-7) was purchased from Titan (Shanghai, China). TMB (AR, 97%, CAS:108-67-8), dimethyl sulfoxide (DMSO, GC, 99.8%, CAS:67-68-5), glutathione (GSH, CAS: 70-18-8), 5,5'-dithiobis (2-nitrobenzoic acid) (DTNB, CAS: 69-78-3), and methylene blue (MB, CAS: 61-73-4) were purchased from Aladdin Reagent (Shanghai, China). H_2O_2 (30%, CAS: 7722-84-1) and KMnO_4 (CAS: 7722-64-7) were supplied by Chuandong Chemical Co., Ltd. (Chongqing, China). Phosphate buffer saline (PBS, Item No.: BF-0011, Beyotime, Shanghai, China), Pluronic® F-127, 5-hydroxyfluorescein resinamide (5-FAM, CAS: 76823-03-5), 2',7'-dichlorodihydrofluorescein diacetate (DCFH-DA, CAS: 4091-99-0), Cell Counting Kit-8 (CCK-8, Item No.: C0039), GSH detection kit (Item No.: S0053), H_2O_2 detection kit (Item No.: S0038), Hoechst 33342 (Item No.: C1025) were purchased from Beyotime (Shanghai, China). Annexin V-fluorescein isothiocyanate/propidium iodide (V-FITC/PI) apoptosis detection kit (Item No.: C1062M) was obtained from Solarbio (Beijing, China). Deionized (DI) water (CAS: 7732-18-5) was used in all preparation processes from the purification system (Synergy, Millipore, MA). Other materials include: TMB (CAS:108-67-8, Aladdin Reagent, Shanghai, China); CPT (CAS: 7689-03-4, Aladdin Reagent, Shanghai, China); potassium permanganate solution (CAS: 7722-64-7, Aladdin Reagent, Shanghai, China); portable dissolved oxygen meter (ST300D, OHAUS, Changzhou, China); dialysis bags (Item No.: MD1444, Yunaye Reagent, Shanghai, China); (UV-Vis)-NIR spectrophotometer (UV-1800, Shimadzu, Japan); well plates (Item No.: 11510, Titan, Shanghai, China); flow cytometry (NovoCyte TM 2060R, USA).

Preparation of MPDA-CPT- MnO_2 nanocomposites

For the preparation of MPDA nanoparticles, 0.36 g of Pluronic® F-127 and 834 μL of TMB were dissolved in a mixture of H_2O (65 mL) and ethanol (60 mL) under stirring. After 30 min, 90 mg of Tris and 60 mg of dopamine hydrochloride were added successively into the mixture. The reaction was performed for 24 h at 30°C and the product pellet was then isolated by centrifugation (8,000 rpm) and washed with ethanol five times.

For CPT loading, 1 mg/mL MPDA aqueous solution and 0.5 mg/mL CPT in DMSO solution were stirred for 24 h under dark conditions, and the product pellets were separated by centrifugation and washed twice with DI water. For MnO_2 coating, 1 mg/mL MPDA-CPT aqueous solution and 0.1 mg/mL potassium permanganate solution were reacted in a water bath at 40°C for 3 h. The product pellets were separated by centrifugation and washed with DI water. The products were dispersed in an aqueous and stored at 4°C. For comparison, MPDA- MnO_2 without CPT loading was also prepared using the same method.

Photothermal performance evaluation

A series of aqueous solutions of MPDA-CPT- MnO_2 nanocomposites in a concentration gradient (0, 100, 200, 300, and 400 ppm) were irradiated with an 808 nm laser (5 min, 1.0 W/cm^2) to record the temperature values. The aqueous solution of MPDA-CPT- MnO_2 nanocomposites and MPDA nanoparticles (400 ppm) was irradiated with the same laser (10 min, 1.0 W/cm^2) and cooled for 20 min. Their photothermal stability was also tested by six repeated cycles of laser on/off process.

O₂ generation assay

To verify the O₂ production capacity, H₂O₂ (100 mmol/L) was added to an aqueous solution of MPDA-CPT-MnO₂ nanocomposites (0.2 mg/mL). The concentration of O₂ generated was determined by a portable dissolved oxygen meter.

CPT release test

MPDA-CPT and MPDA-CPT-MnO₂ nanocomposites (0.5 mg/mL, 2 mL) were packed into dialysis bags (molecular weight = 8,000–14,000) and immersed in the PBS (pH 6.4, 100 mL) at 37°C under the protection from light. At various time points, the dialysate (1 mL) was taken and the absorption at 369 nm was measured by spectrophotometer (UV-1800, Shimadzu). An equal volume of fresh buffer was replenished to maintain the total volume unchanged.

GSH consumption assay

The solutions of MPDA-CPT-MnO₂ nanocomposites with concentrations of 0, 50, 100, 200, 300, and 400 ppm were added to the GSH PBS solution (1 mmol/L, pH 7.4). After reacted for 6 h, 0.9 mL of supernatant was collected and mixed with DTNB solution (50 µL, 5 mg/mL), which can act as the GSH probe [47]. After reacting for 30 min, the absorbance of the supernatant at 412 nm was measured by an ultraviolet-visible (UV-Vis)-NIR spectrophotometer.

•OH detection assay

The mixture of H₂O₂ (20 mmol/L), MB (0.1 mg/mL), and sodium bicarbonate (100 mmol/L, CAS: 144-55-8) was prepared. The solutions of MPDA-CPT-MnO₂ nanocomposites with final concentrations at 0, 20, 40, 60, 80, and 100 ppm were added to the above mixtures and reacted for 1 h. Then, the mixture (1 mL) was centrifuged to obtain the supernatant for UV-Vis-NIR measurement to determine the absorbance at 664 nm.

Cellular uptake assay

4T1 cells were inoculated in 12-well plates (1.0 × 10⁵ per well) and incubated for 12 h. After co-incubation of the cells with the obtained MPDA-CPT-MnO₂ nanocomposites for 1, 3, and 6 h, the cells were washed three times with PBS. The cell uptake behavior was analyzed by flow cytometry (NovoCyte, ACEA). In addition, fluorescent images were captured by confocal laser scanning microscopy [(CLSM) 780, CarlZeiss, Germany].

***In vitro* cytotoxicity assay**

4T1 cells were inoculated in 96-well plates (1.5 × 10⁴ per well) and incubated for 12 h. The cells were then co-incubated with different products for 24 h. Afterward, the cells were washed 3 times with PBS and incubated with 100 µL of medium containing 10 µL of CCK-8 reagent for 30 min. Finally, cell viability was assessed and recorded by a microplate reader (SPARK 10M, Tecan). To study the PTT effect, the cells in corresponding groups were treated with laser irradiation (808 nm, 5 min, 1.0 W/cm²) and the cell viability was measured using the same method.

Intracellular H₂O₂ and GSH measurement

4T1 cells were inoculated in 6-well plates (5.0 × 10⁵ per well) and incubated for 12 h. The cells were then co-incubated with PBS, MPDA, MPDA-MnO₂, and MPDA-CPT-MnO₂ for 6 h. The concentration of all the nanocomposites was kept at 200 ppm. After that, the cells were collected and washed with PBS. The intracellular H₂O₂ and GSH levels were tested using the H₂O₂ detection kit and GSH detection kit, respectively.

Intracellular reactive oxygen species detection

4T1 cells were inoculated in 12-well plates (1.0 × 10⁵ per well) and incubated for 12 h. The cells were then co-incubated with different products (200 ppm) for 6 h. Afterward, the cells were washed 3 times with PBS and stained with DCFH-DA as a reactive oxygen species (ROS) probe for 30 min. Finally, fluorescent images were collected by CLSM.

Apoptosis assay

4T1 cells were inoculated in 12-well plates (1.0×10^5 per well) and incubated for 12 h. The cells were then co-incubated with different products (200 ppm) for 24 h. Afterward, the cells were washed 3 times with PBS. The cells were treated according to the apoptosis kit instructions and finally processed by flow cytometry.

Results

Characterization

Transmission electron microscopy (TEM) image revealed that MPDA showed a regular porous structure with a uniform diameter of around 200 nm (Figure 2a). After CPT loading and MnO_2 coating, the porous structures were invisible, indicating the success of surface coating (Figure 2b). Energy dispersive spectrometer (EDS) mapping analysis revealed the co-existence of C, O, and Mn elements in the formed nanocomposites (Figure 2c). The X-ray photoelectron spectroscopy (XPS) spectrum of Mn 2p displayed two peaks at 652.78 eV and 641.08 eV, corresponding to the Mn(IV) $2p_{1/2}$ and Mn(IV) $2p_{3/2}$ spin-orbit peaks of MnO_2 , respectively (Figure 2d). The content of Mn was measured by inductively coupled plasma-optical emission spectrometry (ICP-OES) to be 9.64% in the final MPDA-CPT- MnO_2 nanocomposites. The Fourier transform infrared (FTIR) spectra of the obtained products demonstrated the successful loading of CPT and coating of the MnO_2 shell on the MPDA surface (Figure 2e) [48, 49]. The UV-Vis spectrum of MPDA showed no obvious peak (Figure 2f). After CPT loading, a typical peak at 369 nm was detected, indicating the loading of the CPT drug. The loading content was calculated to be 21.4% according to its standard curve. The mean hydrodynamic diameter of MPDA was tested to be 210.5 nm with a polydispersity of 11.7, which increased to around 270.1 nm for the final MPDA-CPT- MnO_2 nanocomposites (Figure 2g). In addition, the zeta potential of the products kept similar around -20.0 mV (Figure 2h). The formed MPDA-CPT- MnO_2 nanocomposites could disperse well in DI water, PBS (pH 7.4), and fetal bovine serum (FBS) during 48 h, indicating their good stability under physiological conditions (Figure 2i).

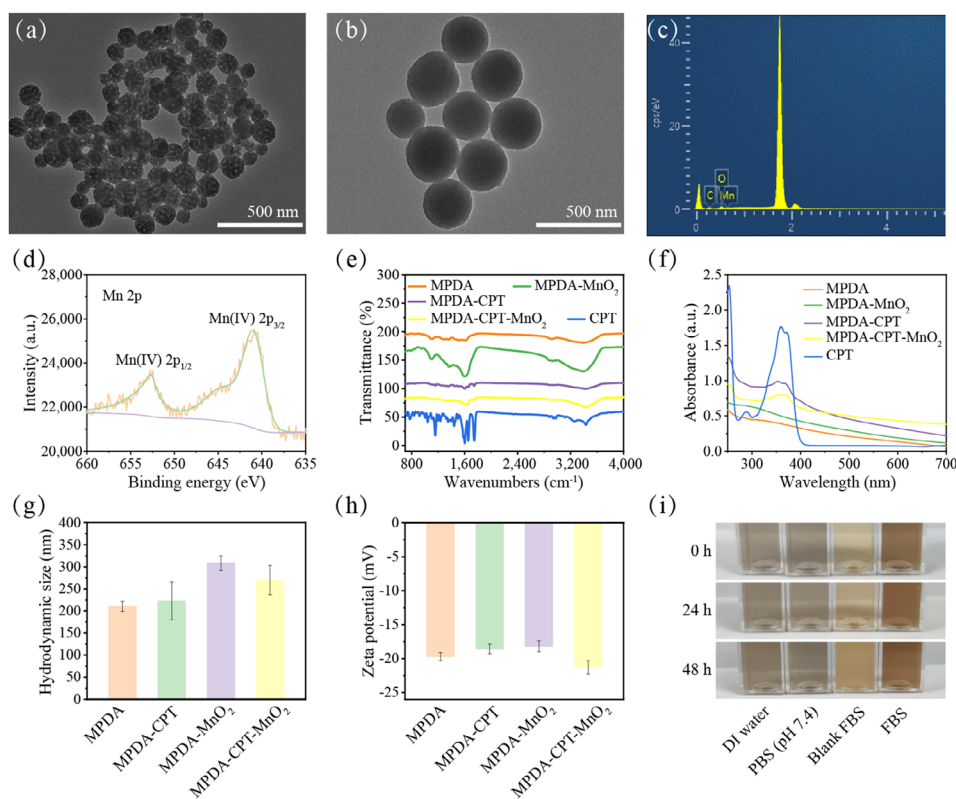


Figure 2. Synthesis and characterization of MPDA-CPT- MnO_2 NPs. TEM images of (a) MPDA and (b) MPDA-CPT- MnO_2 ; (c) EDS mapping analysis of MPDA-CPT- MnO_2 nanocomposites; (d) the high-resolution XPS spectrum of Mn 2p in MPDA-CPT- MnO_2 nanocomposites; (e) FTIR spectra of the obtained products and free CPT; (f) UV-Vis spectra; (g) hydrodynamic size; (h) zeta potential of MPDA, MPDA-CPT, MPDA- MnO_2 , and MPDA-CPT- MnO_2 ; (i) the digital photos of MPDA-CPT- MnO_2 nanocomposites when dispersed in DI water, PBS (pH 7.4), and FBS at 0, 24, and 48 h; CPS: counts per second

Photothermal performance evaluation

The solutions of MPDA-CPT-MnO₂ nanocomposites displayed elevated temperature curves during 5 min laser irradiation, showing a positive correlation with the nanocomposite concentration (Figure 3a). For 400 ppm condition, the solution temperature increased from 25.1°C to 45.2°C after 5 min laser irradiation. The photothermal reproducibility of MPDA-CPT-MnO₂ nanocomposites was assessed under 808 nm laser irradiation (Figure 3b). The photothermal conversion efficiencies of MPDA-CPT-MnO₂ nanocomposites and MPDA nanoparticles were calculated by linear fitting calculations to be 31.5% and 32.3%, respectively (Figure 3c-f).

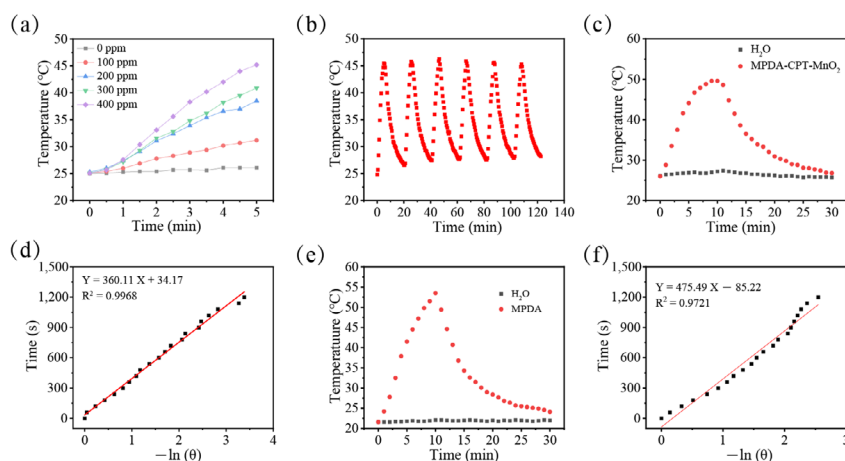


Figure 3. Photothermal performance evaluation. (a) Temperature data of MPDA-CPT-MnO₂ nanocomposite solutions with different concentrations under laser irradiation; (b) the temperature curve of 400 ppm MPDA-CPT-MnO₂ nanocomposite aqueous solution during six lasers on/off cycles; the heating-cooling curve of (c) 400 ppm MPDA-CPT-MnO₂ nanocomposite aqueous solution; (d) was the linear time data versus $-\ln(\theta)$ obtained from the cooling period in (c); (e) 400 ppm MPDA nanoparticle aqueous solution during 30 min; (f) were the linear time data versus $-\ln(\theta)$ obtained from the cooling period in (e)

Stimuli-responsive performance and ROS production detection

As shown in Figure 4a, MPDA-CPT-MnO₂ nanocomposites can react with H₂O₂ to produce O₂, which can further alleviate the drug resistance of tumor cells. Then, the loaded CPT was released from the nanocomposites (Figure 4b). When compared to the un-coated nanocomposites (MPDA-CPT), the release of CPT from MPDA-CPT-MnO₂ nanocomposites was postponed. The production of \cdot OH was detected using MB as a probe. The characteristic absorption peak of MB was found to gradually disappear with the increase of nanocomposite concentration, and meanwhile, the color changed from blue to colorless (Figure 4c). DTNB was used as the probe to detect the depletion of GSH (Figure 4d). The characteristic peak was detected to decrease with the increase of nanocomposite concentration, demonstrating the redox reaction-caused GSH depletion.

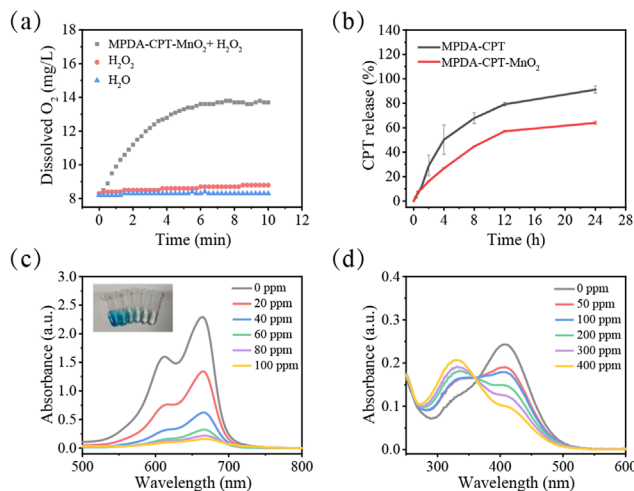


Figure 4. *In vitro* performance investigation. (a) O₂ production curves of MPDA-CPT-MnO₂ nanocomposites in the presence of H₂O₂ at room temperature; (b) CPT release curves from MPDA-CPT and MPDA-CPT-MnO₂ nanocomposites in pH 6.4 buffer

solution; (c) UV-Vis spectra and (inset) digital photo for $\cdot\text{OH}$ detection using MB as the probe in the presence of different concentrations of MPDA-CPT-MnO₂ nanocomposites; (d) UV-Vis spectra for GSH detection using DTNB as the probe in the presence of different concentrations of MPDA-CPT-MnO₂ nanocomposites

Cellular uptake

First, the cellular internalization ability of MPDA-CPT-MnO₂ nanocomposites was characterized. The nanocomposites were fluorescence-labeled using 5-FAM and co-cultured with 4T1 cells. It was found that the fluorescence signal gradually increased with the nanocomposite concentration and incubation time (Figure 5a–c). As shown in the CLSM images, the cells at 6 h showed the strongest green fluorescence signal (Figure 5d).

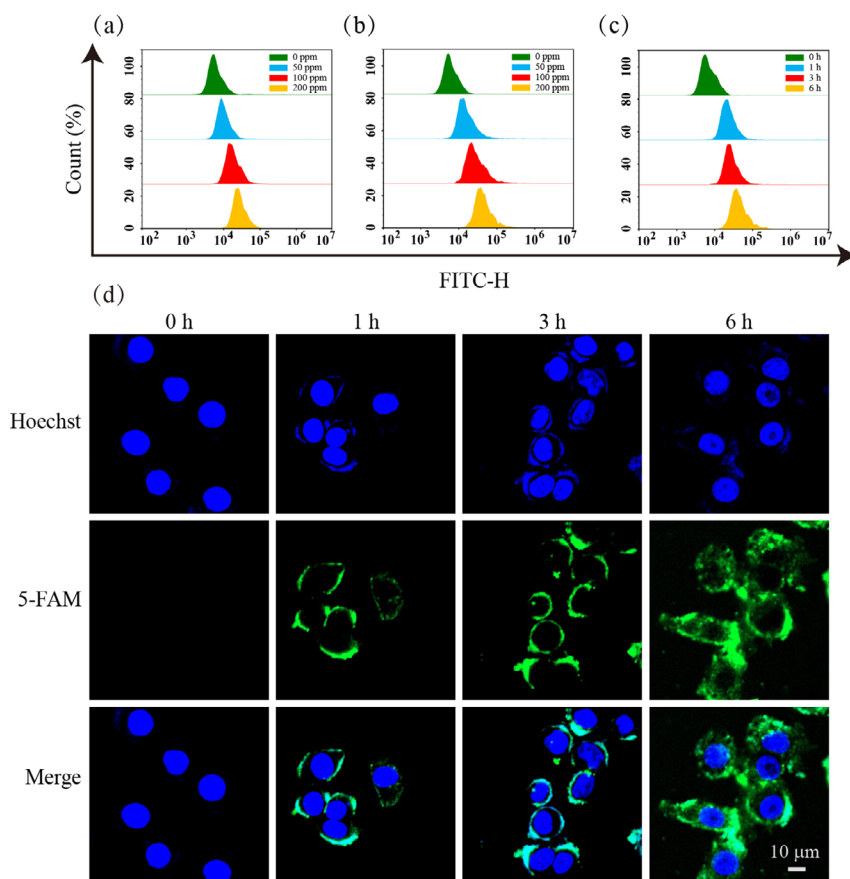


Figure 5. Cellular uptake performance. Flow cytometry curves of 4T1 cells after co-incubation with MPDA-CPT-MnO₂ nanocomposites of different concentrations (0, 50, 100, and 200 ppm) for (a) 3 h and (b) 6 h; (c) flow cytometry curves of 4T1 cells after co-incubation with 200 ppm MPDA-CPT-MnO₂ nanocomposites for different time points (0, 1, 3, and 6 h); (d) CLSM images of 4T1 cells after co-incubation with 200 ppm MPDA-CPT-MnO₂ nanocomposites for different time points (0, 1, 3, and 6 h); H: height

Cell viability assay and mechanism exploration

As shown in Figure 6a, the cells in the MPDA group displayed similar viability data (0–200 ppm) to that of the control group, revealing the good cytocompatibility of the formed MPDA nanoparticles. A slight influence on cell viability was observed when the concentration of MPDA nanoparticles reached 300 ppm and above. The cells in the MPDA-MnO₂ and MPDA-CPT groups decreased due to the therapeutic effect of CDT and CT, respectively. When treated with MPDA-CPT-MnO₂ nanocomposites, the cell viability decreased significantly, which was further decreased under laser irradiation. At 300 ppm and 400 ppm conditions, the cell viability data in the MPDA-CPT-MnO₂ plus laser group displayed great significant difference to all other groups.

Then, the therapeutic mechanism was explored. The H₂O₂ levels in cells after treatments were shown in Figure 6b. Then, DCFH-DA was employed as a fluorescent indicator to measure the intracellular ROS level. The fluorescence images showed that 4T1 cells cultured with MPDA-MnO₂ nanocomposites exhibited higher green fluorescence than that of the PBS group, demonstrating the production of ROS (Figure 6c). It was detected that the GSH level decreased significantly in the presence of MnO₂ (Figure 6d).

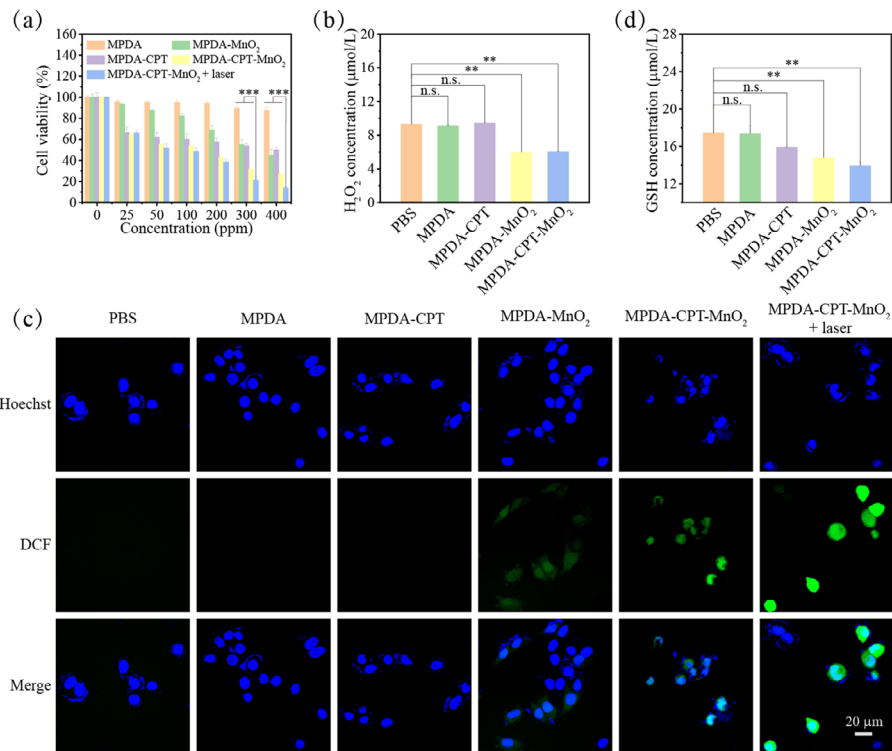


Figure 6. Intracellular performance evaluation. (a) 4T1 cell viability data after 24 h treatment with different samples without or with laser irradiation; (b) intracellular H₂O₂ level measurements after incubation with MPDA, MPDA-CPT, MPDA-MnO₂, or MPDA-CPT-MnO₂ nanocomposites; (c) DCFH-DA kit for the detection of intracellular ROS levels in 4T1 cells after different treatments; (d) intracellular GSH level measurements after incubation with MPDA, MPDA-CPT, MPDA-MnO₂, or MPDA-CPT-MnO₂ nanocomposites (***P* < 0.01 and ****P* < 0.001 and n.s.: non-significance; DCF: 2',7'-dichlorofluorescein

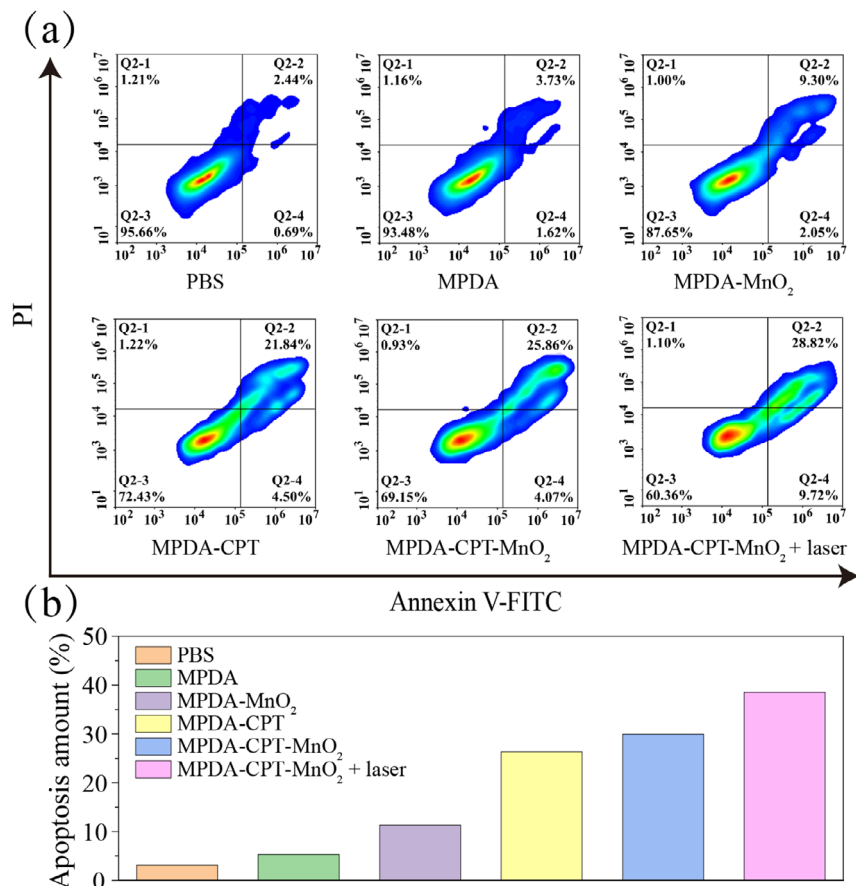


Figure 7. Apoptosis analysis. (a) Apoptosis data; (b) the corresponding quantitative histogram of 4T1 cells measured by flow cytometry after treatment with MPDA, MPDA-MnO₂, MPDA-CPT, MPDA-CPT-MnO₂, or MPDA-CPT-MnO₂ nanocomposites. The corresponding group was laser irradiated

In addition, the apoptosis percentages after different treatments were tested using an apoptosis kit (Figure 7). It was found that the apoptosis percentages in the MPDA-MnO₂ and MPDA-CPT groups were 11.35% and 26.34%, respectively, which increased to 29.93% after MPDA-CPT-MnO₂ nanocomposite treatment. The highest apoptosis percentage was detected to be 38.54% in the MPDA-CPT-MnO₂ plus laser group.

Discussion

MPDA nanoparticles were prepared by self-polymerization of dopamine hydrochloride using Pluronic® F-127 as surfactant and TMB as templating agent. MPDA nanoparticles own abundant surface phenyls, amino, and hydroxyl groups, endowing them with the excellent capability to load various chemical drugs through π - π stacking and/or hydrogen bond interaction [50]. The MnO₂ coating layer displayed negligible influence on the absorption spectrum. Through characterization, the MPDA-CPT-MnO₂ nanocomposites were successfully formed with good stability.

The photothermal property of MPDA-CPT-MnO₂ nanocomposites at different concentrations was investigated using an 808 nm laser. They showed good photothermal performance. The photothermal reproducibility of MPDA-CPT-MnO₂ nanocomposites was assessed to be excellent. These photothermal tests indicated that the MnO₂ coating displayed no significant effect on the photothermal conversion efficiency of MPDA nanoparticles and the obtained MPDA-CPT-MnO₂ nanocomposites owned good photothermal performance.

The coated MnO₂ layer was acid-responsive, which can degrade to release O₂ in the presence of H₂O₂. The MnO₂ layer was successfully coated onto the surface of nanocomposites that can prevent drug leakage. During this degradation process, Mn²⁺ was generated and can act as a Fenton-like agent to produce highly toxic •OH. After the Fenton-like reaction, Mn²⁺ was converted into Mn⁴⁺, which tended to proceed redox reaction with GSH to generate Mn²⁺ and deplete GSH. It was demonstrated that the production of •OH by the formed MPDA-CPT-MnO₂ nanocomposites was in a concentration-dependent manner.

4T1 cells were used to assess the performance of MPDA-CPT-MnO₂ nanocomposites at the cellular level. The data demonstrated that MPDA-CPT-MnO₂ nanocomposites can be effectively internalized by 4T1 cells. The CCK-8 assay was then used to assess the survival rate of 4T1 cells under different treatments. It was found that MPDA nanoparticles displayed good cytocompatibility in the low concentration range (0–200 ppm). Further data demonstrated the high efficacy of collaborative CT/PTT/CDT for tumor cell killing.

The generated Mn²⁺ can act as a Fenton-like agent to convert H₂O₂ into •OH. The H₂O₂ levels in the MPDA-MnO₂ and MPDA-CPT-MnO₂ groups decreased greatly when compared to the PBS control group. For intracellular ROS detection, the fluorescence signal in the MPDA-CPT-MnO₂ nanocomposite group became stronger, indicating the CPT-induced apoptosis-related ROS production. The fluorescence signal in the MPDA-CPT-MnO₂ plus laser group was stronger than all other groups, suggesting that the efficiency of ROS production can be enhanced by the photothermal effect. After the Fenton-like reaction, the produced Mn⁴⁺ could react with GSH through a redox reaction to produce Mn²⁺ and deplete GSH. This could disrupt the reducing capacity of tumor cells and benefit the production of ROS. Further cell viability data demonstrated that the formed MPDA-CPT-MnO₂ nanocomposites could cause 4T1 cell apoptosis effectively under laser irradiation.

In conclusion, MPDA-CPT-MnO₂ nanocomposites were prepared for collaborative CT/PTT/CDT against tumor cells. The formed MPDA-CPT-MnO₂ nanocomposites displayed uniform morphology with a hydrodynamic diameter of 270.1 nm. The loading content of CPT was around 21.4%. They displayed good photothermal conversion effect and photothermal stability. In the presence of acid and H₂O₂, MPDA-CPT-MnO₂ nanocomposites degraded to produce O₂, release CPT, and generate Mn²⁺ as the Fenton-like agents. The formed MPDA-CPT-MnO₂ nanocomposites can be up-taken by 4T1 cells effectively. They can produce ROS and deplete GSH in 4T1 cells, finally causing cell apoptosis. Cell viability revealed that the developed MPDA-CPT-MnO₂ nanocomposites can kill tumor cells with high efficacy through a collaborative strategy.

Abbreviations

•OH: hydroxyl radicals
CCK-8: Cell Counting Kit-8
CDT: chemodynamic therapy
CLSM: confocal laser scanning microscopy
CPT: camptothecin
CT: chemotherapy
DCFH-DA: 2',7'-dichlorodihydrofluorescein diacetate
DI: deionized
DTNB: 5,5'-dithiobis (2-nitrobenzoic acid)
GSH: glutathione
H₂O₂: hydrogen peroxide
KMnO₄: potassium permanganate
MB: methylene blue
MnO₂: manganese dioxide
MPDA: mesoporous polydopamine
NIR: near-infrared
PBS: phosphate buffer saline
Pluronic® F-127: poly(ethylene glycol)-*block*-poly(propylene glycol)-*block*-poly(ethylene glycol)
PTT: photothermal therapy
ROS: reactive oxygen species
TMB: trimethylbenzene
UV-Vis: ultraviolet-visible

Declarations

Author Contributions

YO: Data curation, Formal Analysis, Writing—original draft. YC: Formal Analysis, Investigation. TX: Formal Analysis, Investigation. YS: Formal Analysis, Investigation. SZ: Formal Analysis, Investigation. CC: Formal Analysis, Investigation. YT: Formal Analysis, Investigation. LH: Formal Analysis, Investigation. HL: Conceptualization, Funding acquisition, Writing—review & editing.

Conflicts of interest

The authors declare that they have no conflicts of interest.

Ethical approval

Not applicable.

Consent to participate

Not applicable.

Consent to publication

Not applicable.

Availability of data and materials

Not applicable.

Funding

This research was funded by the National Natural Science Foundation of China [No. 51703184]. The funders had no role in study design, data collection and analysis, decision to publish, or preparation of the manuscript.

Copyright

© The Author(s) 2023.

References

1. Li Z, Yu XF, Chu PK. Recent advances in cell-mediated nanomaterial delivery systems for photothermal therapy. *J Mat Chem B*. 2018;6:1296–311.
2. Liu SW, Wang L, Lin M, Liu Y, Zhang LN, Zhang H. Tumor photothermal therapy employing photothermal inorganic nanoparticles/polymers nanocomposites. *Chin J Polym Sci*. 2019;37:115–28.
3. Zeng W, Zhang H, Yuan X, Chen T, Pei Z, Ji X. Two-dimensional nanomaterial-based catalytic medicine: theories, advanced catalyst and system design. *Adv Drug Deliv Rev*. 2022;184:114241.
4. Kang Y, Kong N, Ou M, Wang Y, Xiao Q, Mei L, et al. A novel cascaded energy conversion system inducing efficient and precise cancer therapy. *Bioact Mater*. 2022;20:663–76.
5. Ji X, Kang Y, Ouyang J, Chen Y, Artzi D, Zeng X, et al. Synthesis of ultrathin biotite nanosheets as an intelligent theranostic platform for combination cancer therapy. *Adv Sci*. 2019;6:1901211.
6. Kong N, Zhang H, Feng C, Liu C, Xiao Y, Zhang X, et al. Arsenene-mediated multiple independently targeted reactive oxygen species burst for cancer therapy. *Nat Commun*. 2021;12:4777.
7. Jaque D, Martínez Maestro L, del Rosal B, Haro-Gonzalez P, Benayas A, Plaza JL, et al. Nanoparticles for photothermal therapies. *Nanoscale*. 2014;6:9494–530.
8. He T, Luo Y, Zhang Q, Men Z, Su T, Fan L, et al. Hyalase-mediated cascade degradation of a matrix barrier and immune cell penetration by a photothermal microneedle for efficient anticancer therapy. *ACS Appl Mater Interfaces*. 2021;13:26790–9.
9. Li X, Lovell JF, Yoon J, Chen X. Clinical development and potential of photothermal and photodynamic therapies for cancer. *Nat Rev Clin Oncol*. 2020;17:657–74.
10. Han HS, Choi KY. Advances in nanomaterial-mediated photothermal cancer therapies: toward clinical applications. *Biomedicines*. 2021;9:305.
11. Mortezaee K, Narmani A, Salehi M, Bagheri H, Farhood B, Haghi-Aminjan H, et al. Synergic effects of nanoparticles-mediated hyperthermia in radiotherapy/chemotherapy of cancer. *Life Sci*. 2021;269:119020.
12. Li X, Sun H, Li H, Hu C, Luo Y, Shi X, et al. Multi-responsive biodegradable cationic nanogels for highly efficient treatment of tumors. *Adv Funct Mater*. 2021;31:2100227.
13. Zeng X, Luo M, Liu G, Wang X, Tao W, Lin Y, et al. Polydopamine-modified black phosphorous nanocapsule with enhanced stability and photothermal performance for tumor multimodal treatments. *Adv Sci*. 2018;5:1800510.
14. Sun H, Yu T, Li X, Lei Y, Li J, Wang X, et al. Second near-infrared photothermal-amplified immunotherapy using photoactivatable composite nanostimulators. *J Nanobiotechnol*. 2021;19:433.
15. Li J, Yu X, Jiang Y, He S, Zhang Y, Luo Y, et al. Second near-infrared photothermal semiconducting polymer nanoadjuvant for enhanced cancer immunotherapy. *Adv Mater*. 2021;33:e2003458.
16. Yang Y, Zhu W, Dong Z, Chao Y, Xu L, Chen M, et al. 1D coordination polymer nanofibers for low-temperature photothermal therapy. *Adv Mater*. 2017;29:1703588.
17. Tang Z, Zhang H, Liu Y, Ni D, Zhang H, Zhang J, et al. Antiferromagnetic pyrite as the tumor microenvironment-mediated nanoplatform for self-enhanced tumor imaging and therapy. *Adv Mater*. 2017;29:1701683.

18. Ou YC, Webb JA, Faley S, Shae D, Talbert EM, Lin S, et al. Gold nanoantenna-mediated photothermal drug delivery from thermosensitive liposomes in breast cancer. *ACS Omega*. 2016;1:234–43.
19. Yang Z, Luo Y, Hu Y, Liang K, He G, Chen Q, et al. Photothermo-promoted nanocatalysis combined with H₂S-mediated respiration inhibition for efficient cancer therapy. *Adv Funct Mater*. 2020;31:2007991.
20. Qu Y, Chu B, Wei X, Lei M, Hu D, Zha R, et al. Redox/pH dual-stimuli responsive camptothecin prodrug nanogels for “on-demand” drug delivery. *J Control Release*. 2019;296:93–106.
21. Thomas CJ, Rahier NJ, Hecht SM. Camptothecin: current perspectives. *Bioorg Med Chem*. 2004;12:1585–604.
22. Srivastava V, Negi AS, Kumar JK, Gupta MM, Khanuja SP. Plant-based anticancer molecules: a chemical and biological profile of some important leads. *Bioorg Med Chem*. 2005;13:5892–908.
23. Ray CA, Hashimoto Y, Herrador R, Neelsen KJ, Fachinetti D, Bermejo R, et al. Topoisomerase I poisoning results in PARP-mediated replication fork reversal. *Nat Struct Mol Biol*. 2012;19:417–23.
24. Behera A, Padhi S. Passive and active targeting strategies for the delivery of the camptothecin anticancer drug: a review. *Environ Chem Lett*. 2020;18:1557–67.
25. Beretta GL, Gatti L, Perego P, Zaffaroni N. Camptothecin resistance in cancer: insights into the molecular mechanisms of a DNA-damaging drug. *Curr Med Chem*. 2013;20:1541–65.
26. Cheetham AG, Zhang P, Lin YA, Lock LL, Cui H. Supramolecular nanostructures formed by anticancer drug assembly. *J Am Chem Soc*. 2013;135:2907–10.
27. Liao L, Liu J, Dreaden EC, Morton SW, Shopsowitz KE, Hammond PT, et al. A convergent synthetic platform for single-nanoparticle combination cancer therapy: ratiometric loading and controlled release of cisplatin, doxorubicin, and camptothecin. *J Am Chem Soc*. 2014;136:5896–9.
28. Zhu M, Shi Y, Shan Y, Guo J, Song X, Wu Y, et al. Recent developments in mesoporous polydopamine-derived nanoplatforms for cancer theranostics. *J Nanobiotechnol*. 2021;19:387.
29. Yue Y, Zhao X. Melanin-like nanomedicine in photothermal therapy applications. *Int J Mol Sci*. 2021;22:399.
30. Wang Z, Zou Y, Li Y, Cheng Y. Metal-containing polydopamine nanomaterials: catalysis, energy, and theranostics. *Small*. 2020;16:e1907042.
31. Shu G, Chen M, Song J, Xu X, Lu C, Du Y, et al. Sialic acid-engineered mesoporous polydopamine nanoparticles loaded with SPIO and Fe³⁺ as a novel theranostic agent for T1/T2 dual-mode MRI-guided combined chemo-photothermal treatment of hepatic cancer. *Bioact Mater*. 2021;6:1423–35.
32. Zhang L, Yang P, Guo R, Sun J, Xie R, Yang W. Multifunctional mesoporous polydopamine with hydrophobic paclitaxel for photoacoustic imaging-guided chemo-photothermal synergistic therapy. *Int J Nanomed*. 2019;14:8647–63.
33. Yang M, Zhang N, Zhang T, Yin X, Shen J. Fabrication of doxorubicin-gated mesoporous polydopamine nanoplatforms for multimode imaging-guided synergistic chemophotothermal therapy of tumors. *Drug Deliv*. 2020;27:367–77.
34. Zeng W, Zhang H, Deng Y, Jiang A, Bao X, Guo M, et al. Dual-response oxygen-generating MnO₂ nanoparticles with polydopamine modification for combined photothermal-photodynamic therapy. *Chem Eng J*. 2020;389:124494.
35. Song T, Liao Y, Zuo Q, Liu N, Liu Z. MnO₂ nanoparticles as a minimalist multimode vaccine adjuvant/delivery system to regulate antigen presenting cells for tumor immunotherapy. *J Mat Chem B*. 2022;10:3474–90.
36. Gao F, Sun M, Zhang J, Chang Y, Gao W, Ma G, et al. Fenton-like reaction and glutathione depletion by chiral manganese dioxide nanoparticles for enhanced chemodynamic therapy and chemotherapy. *J Colloid Interface Sci*. 2022;616:369–78.
37. Ding B, Zheng P, Ma P, Lin J. Manganese oxide nanomaterials: synthesis, properties, and theranostic applications. *Adv Mater*. 2020;32:e1905823.

38. Yang G, Xu L, Chao Y, Xu J, Sun X, Wu Y, et al. Hollow MnO₂ as a tumor-microenvironment-responsive biodegradable nano-platform for combination therapy favoring antitumor immune responses. *Nat Commun.* 2017;8:902.
39. Liang S, Liao G, Zhu W, Zhang L. Manganese-based hollow nanoplatfoms for MR imaging-guided cancer therapies. *Biomater Res.* 2022;26:32.
40. Song M, Liu T, Shi C, Zhang X, Chen X. Bioconjugated manganese dioxide nanoparticles enhance chemotherapy response by priming tumor-associated macrophages toward M1-like phenotype and attenuating tumor hypoxia. *ACS Nano.* 2016;10:633–47. Erratum in: *ACS Nano.* 2016;10:3872.
41. Zhang P, Wu Q, Yang J, Hou M, Zheng B, Xu J, et al. Tumor microenvironment-responsive nanohybrid for hypoxia amelioration with photodynamic and near-infrared II photothermal combination therapy. *Acta Biomater.* 2022;146:450–64.
42. Lin LS, Song J, Song L, Ke K, Liu Y, Zhou Z, et al. Simultaneous Fenton-like ion delivery and glutathione depletion by MnO₂-based nanoagent to enhance chemodynamic therapy. *Angew Chem Int Edit.* 2018;57:4902–6.
43. Gu D, An P, He X, Wu H, Gao Z, Li Y, et al. A novel versatile yolk-shell nanosystem based on NIR-elevated drug release and GSH depletion-enhanced Fenton-like reaction for synergistic cancer therapy. *Colloid Surf B Biointerfaces.* 2020;189:110810.
44. Kang Y, Mao Z, Wang Y, Pan C, Ou M, Zhang H, et al. Design of a two-dimensional interplanar heterojunction for catalytic cancer therapy. *Nat Commun.* 2022;13:2425.
45. Ember E, Rothbart S, Puchta R, van Eldik R. Metal ion-catalyzed oxidative degradation of orange II by H₂O₂. High catalytic activity of simple manganese salts. *New J Chem.* 2009;33:34–49.
46. He T, Jiang C, He J, Zhang Y, He G, Wu J, et al. Manganese-dioxide-coating-instructed plasmonic modulation of gold nanorods for activatable duplex-imaging-guided NIR-II photothermal-chemodynamic therapy. *Adv Mater.* 2021;33:e2008540.
47. Chen L, Mao Z, Wang Y, Kang Y, Wang Y, Mei L, et al. Edge modification facilitated heterogenization and exfoliation of two-dimensional nanomaterials for cancer catalytic therapy. *Sci Adv.* 2022;8:eabo7372.
48. Li S, Lin K, Hu P, Wang S, Zhao S, Gan Y, et al. A multifunctional nanoamplifier with self-enhanced acidity and hypoxia relief for combined photothermal/photodynamic/starvation therapy. *Int J Pharm.* 2022;611:121307.
49. Yang JC, Chen Y, Li YH, Yin XB. Magnetic resonance imaging-guided multi-drug chemotherapy and photothermal synergistic therapy with pH and NIR-stimulation release. *ACS Appl Mater Interfaces.* 2017;9:22278–88.
50. Wang X, Zhang J, Wang Y, Wang C, Xiao J, Zhang Q, et al. Multi-responsive photothermal-chemotherapy with drug-loaded melanin-like nanoparticles for synergetic tumor ablation. *Biomaterials.* 2016;81:114–24.